PUBLICATIONS OF THE ASTRONOMICAL SOCIETY OF THE PACIFIC, 112:966–976, 2000 July

High-Precision Radial Velocity Measurements of Some Southern Stars

JOVAN SKULJAN, JOHN B. HEARNSHAW, AND PETER L. COTTRELL

Department of Physics and Astronomy, University of Canterbury, Private Bag 4800, Christchurch 8020, New Zealand;
j.skuljan@phys.canterbury.ac.nz

Received 2000 February 16; accepted 2000 March 30

ABSTRACT. Precise absolute radial velocities have been obtained at Mount John University Observatory for a number of southern stars, using the 1 m telescope and fiber-fed echelle spectrograph. Only the stars that have been observed three or more times are presented, including 14 IAU standards and 11 program stars. Six echelle orders in the green (5000–5600 Å) are used. Many delicate steps have been undertaken in order to maintain the same conditions in both recording and reducing the spectra over a period of 27 months. The Th-Ar lamp has been used for the wavelength calibration. The absolute radial velocities have been determined by cross-correlation with synthetic spectra computed by R. L. Kurucz. The zero point has been adjusted using blue-sky spectra. An additional strong correlation, between the measured velocities and photon counts in stellar and Th-Ar spectra, has been detected for the PM3000 CCD camera and has been eliminated. A resulting precision of about 20–30 m s^{-1} has been obtained. The overall uncertainty of the absolute radial velocities was estimated to be about 100–200 m s^{-1}. The present paper is a continuation of our recent previous work, including more details on the reduction process and the presentation of the radial velocities for more stars.

1. INTRODUCTION

This paper is part of a larger project started at the University of Canterbury in order to study the reality of the concept of moving groups of stars in our Galaxy (Skuljan, Cottrell, & Hearnshaw 1997; Skuljan, Hearnshaw, & Cottrell 1999c). During the 3 year observing period from 1995 April 24 to 1998 May 3, a total of 1536 radial velocity observations were collected for 432 different objects. Most of the observing time was spent at Mount John University Observatory (MJUO), Lake Tekapo, New Zealand, but a significant number of northern stars were observed from the Dominion Astrophysical Observatory, Victoria, British Columbia, Canada. Some of the results obtained at both observatories were presented at the IAU Colloquium 170 (Skuljan, Hearnshaw, & Cottrell 1999a, 1999b). In the present paper a more detailed presentation of the MJUO echelle observations will be given, including the results for a number of standard and program stars.

2. OBSERVING EQUIPMENT

The MJUO observing equipment for this project was based on the 1 m telescope and the echelle spectrograph. The spectrograph is placed in a separate temperature-controlled room at 25°.0 ± 0°.1 (Cummings 1998), and both the stellar light and the light from calibration lamps is transferred to the spectrograph by a 25 m long and 105 μm thick optical fiber (Hearnshaw 1977; Kershaw & Hearnshaw 1989). Because of the scrambling properties of the fiber feed, the traditional guiding error is largely eliminated. The fiber tips are not polished, but a glycerin drop is inserted between the fiber input and the quartz window in the focal plane of the telescope to ensure a uniform illumination of the fiber entrance. The glycerin drop deteriorates and evaporates slowly, so that it has to be reinserted on a regular basis (typically once a year). A CCD camera is used to record a two-dimensional image of several (six for the PM3000 camera) diffraction orders in the focal plane of the spectrograph.

The spectrograph is based on an echelle grating having 79 grooves mm^{-1}, with a blaze angle of $\theta_B \approx 65°.4$ ($\lambda_B =$ 5480 Å in order 42). Another diffraction grating (150 grooves mm^{-1}, $\lambda_B = 5000$ Å in the first order) is used as a cross-disperser. The collimator and camera are parabolic and spherical mirrors, respectively ($f_{col} = 54$ cm, $f_{cam} = 75$ cm). An additional lens (focal reducer) has been added to the system recently in order to put more echelle orders onto the CCD chip.

Two CCD detectors have been available with the 1 m telescope: a Thomson TH7882 CDA chip (576 × 384 23 μm pixels) incorporated into the Photometrics PM3000 CCD system (Tobin 1992) and a SITe chip (1024 × 1024 24 μm pixels) in the Photometrics Series 200 system. The SITe camera became available only at the end of the observing program, and it was used in the later observing runs (from 1997 September).

TABLE 1

BASIC PARAMETERS FOR THE ECHELLE SPECTRA

Order	Range (Å)	λ_{cen} (Å)	D (pixels Å^{-1})	$\Delta\lambda$ (mÅ)
46.....	5008.3–5030.9	5019.6	25.4	129
45.....	5119.5–5142.7	5131.1	24.8	132
44.....	5235.8–5259.5	5247.6	24.3	135
43.....	5357.5–5381.7	5369.6	23.7	138
42.....	5485.0–5509.8	5497.4	23.2	141
41.....	5618.7–5644.1	5631.4	22.6	145

A typical average FWHM of sharp emission lines in the CCD images (as measured from the Th-Ar spectra) is 3.27 pixels for the PM3000 camera (without the focal reducer) and 2.31 pixels for the SITe chip (with the focal reducer). This is the width of the slit image projected onto the CCD chip and defines the effective resolution of the spectrograph.

The wavelength regions and other characteristics of the observed echelle spectra (PM3000 system without the focal reducer) are given in Table 1. No telluric lines are found in this spectral range. The resolution ($\Delta\lambda$) has been calculated by dividing the FWHM value of 3.27 pixels (as mentioned above) by the dispersion (D). The resolving power ($R = \lambda/\Delta\lambda$) can be calculated by dividing the central wavelength (λ_{cen}) by the resolution ($\Delta\lambda$). A typical value of $R \approx 38{,}900$ is obtained.

It should be pointed out that the instrument used for this work is not new. More details on the particular design can be found in the references mentioned in the beginning of this section. The overall performance of the spectrograph is also discussed in Murdoch, Hearnshaw, & Clark (1993). Our precision is still affected by temperature and pressure changes from one exposure to another and slightly by the guiding error since no double scrambler is used. There are other fiber-fed systems used for radial velocity measurements, such as the ELODIE (Baranne et al. 1996) and AFOE (Brown et al. 1994). A very high precision of 3–10 m s^{-1} was obtained by Marcy, Butler, & Fischer (1999) using a different design (iodine cell) and taking care of the variations of the point-spread function across the CCD.

3. REDUCTION PROCEDURE

All reductions were basically done in ESO-MIDAS, combined with some additional subroutines written in C and FORTRAN (cross-correlation, barycentric correction, etc.). The reduction procedure can be divided into two main stages. During the first stage, the one-dimensional stellar spectrum is produced, so that each echelle order is given as a normalized relative intensity depending on the wavelength. This stage includes the background subtraction, cosmic-ray elimination, order extraction, flat-fielding, wavelength calibration (dispersion solution), and normalization. The second stage is a cross-correlation between the stellar spectrum and the corresponding theoretical (synthetic) spectrum. The radial velocity is derived from the positions of the peaks in the cross-correlation functions, by averaging all echelle orders. An example of this process is given in Figure 1. An appropriate barycentric correction is applied to the final result to eliminate the Earth's motion. Blue-sky spectra are used for the zero-point adjustments. The sky observations are always made approximately at the same angular separation from the Sun so that the effect of changeable line profiles (Gray, Tycner, & Brown 2000) is avoided.

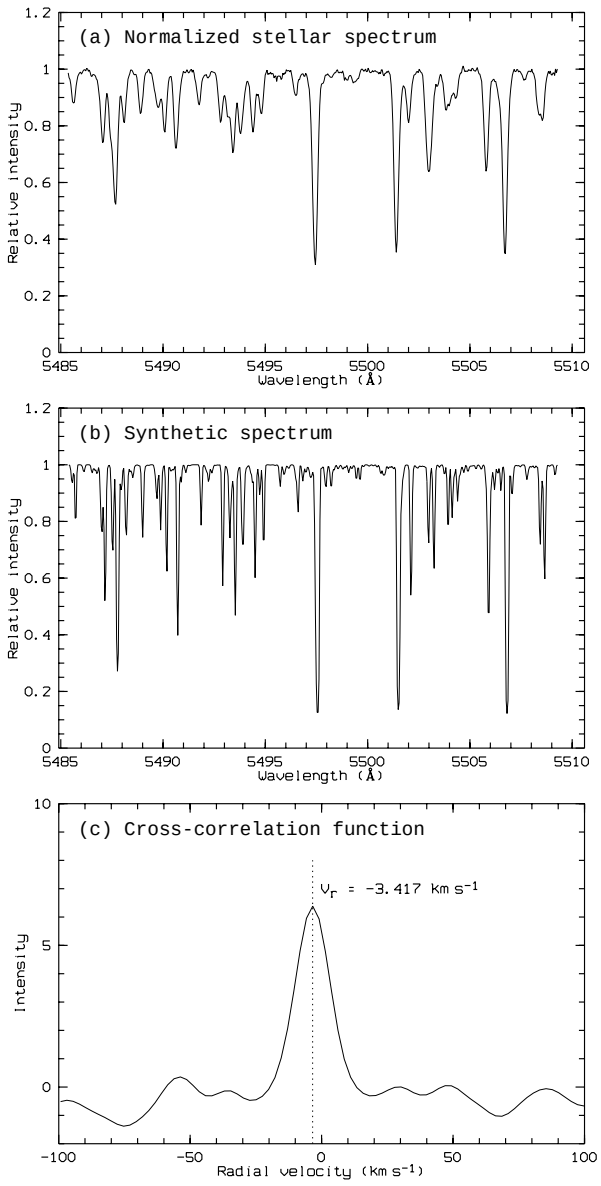

FIG. 1.—The radial velocity is obtained by cross-correlation between the observed stellar spectrum and a synthetic one. An image of β Corvi is used. Only order 42 is shown.

Only some of the most important reduction steps (the wavelength calibration and the cross-correlation with the synthetic spectra) will be discussed here in more detail.

3.1. The Wavelength Calibration

The Th-Ar spectrum is used for the wavelength calibration. All six echelle orders are treated simultaneously so that a two-dimensional polynomial solution is found in a form $x = f(n, \lambda)$, where x is the pixel position of a spectral line on the CCD image, n is the order number, and λ is the corresponding laboratory wavelength. The calibration spectra are taken immediately before and after the stellar exposure and an average solution is computed.

In order to maintain the highest possible stability of the dispersion solutions in the Th-Ar spectra, the following points have been adopted:

1. Only well-defined and stable spectral lines are used (i.e., ones that give reliable, stable centers when measured repeatedly).
2. The same set of spectral lines is always used. Numerous tests performed on the Th-Ar spectra demonstrate that even a small change in the line selection criteria (i.e., rejecting some lines and accepting some others) can result in a different dispersion solution.
3. The same portions of the spectral lines to the nearest pixel are always used to define the line centers. A Gaussian profile (with equal weights on all pixels) is fitted to every spectral line, but the first and last pixels for the fit are set for each line separately, depending on other nearby lines.

For these reasons it was necessary to abandon the standard MIDAS wavelength calibration procedure and a new one was developed, using a fixed table of carefully selected spectral lines. The selection process consists of three major steps:

1. From many Th-Ar spectra, taken on the same observing night, the mean central intensity for each line is defined. Those lines that show unacceptable scatter from one image to another are rejected.
2. The mean central pixel position is defined for each spectral line, using the same set of images. Those lines that show unacceptable scatter are rejected.
3. The dispersion solution is computed. Those lines that deviate significantly from the fitted position (heavily blended lines) are rejected.

A result of this selection process for the PM3000 system is presented in Figure 2. There are 72 preliminary lines when all six echelle orders are considered together. It is evident from Figure 2*a* that the weaker lines are more scattered in their intensities than the stronger ones. The scatter (standard deviation) has been computed from many Th-Ar images. The images have first been rescaled to the same mean intensity. In this way, any real fluctuations in the Th-Ar lamp brightness from one image to another have been eliminated,[1] and only the random errors of the fitting process remain. It is interesting to note that all thorium lines (*black dots*) follow the same general trend, with a

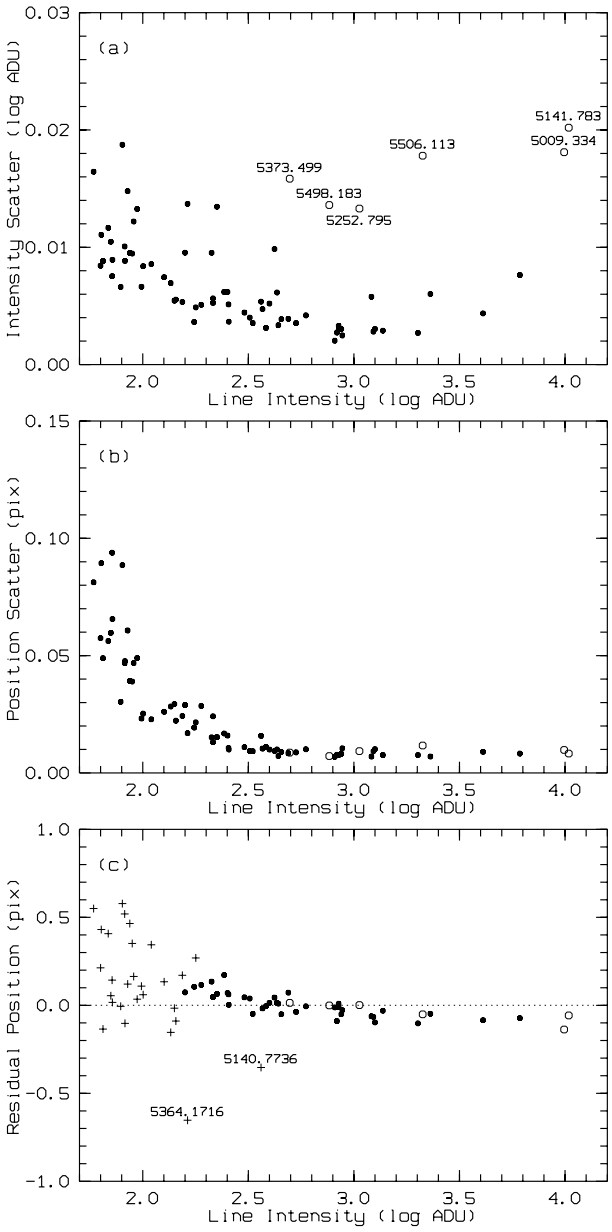

FIG. 2.—Some properties of spectral lines selected for the wavelength calibration: (*a*) intensity scatter for thorium (*black dots*) and argon (*open circles*), (*b*) position scatter, and (*c*) residual positions. Crosses are used to mark the spectral lines that are not used for wavelength calibration.

[1] In order to minimize these fluctuations, the lamp was kept on continuously during an observing night.

scatter decreasing slowly, as the line strength increases. On the other hand, all argon lines (*open circles*) seem to exhibit a different behavior, with a higher scatter for the same central intensity. It is possible that the argon source is actually less stable compared to the thorium source within the same lamp.

The stability of central positions (Fig. 2*b*) is used as the main criterion for accepting or rejecting a given spectral line. The scatter (standard deviation) has been computed from many Th-Ar images, but any global shifts from one image to another have first been eliminated. The correlation between the scatter and the intensity is even more obvious and regular than in the case of intensity scatter (Fig. 2*a*). All spectral lines (argon included) stronger than about 300 ADU (2.5 in logarithmic units) are extremely stable in their positions, with a standard deviation of only ~ 0.01 pixel. However, weaker lines demonstrate a steep increase in the scatter, up to about 0.1 pixel. If one excludes the weakest lines from the wavelength calibration process, the stability of the dispersion solution will be improved, as well as the precision of the radial velocities.

The third plot (Fig. 2*c*) demonstrates the residuals as computed from a two-dimensional parabolic fit,[2] $x = P_{2,2}(n, \lambda)$, to the spectral lines. As a source of the thorium laboratory wavelengths, the Atlas of the Thorium Spectrum by Palmer & Engleman (1983) with eight significant digits was used. A limited number of strong argon lines have been taken from Reader & Corliss (1980) with seven significant digits. Each point in Figure 2*c* represents a difference between the measured pixel position and the fitted pixel position. Only the 50 strongest lines (*black dots and open circles*) have been used for the least-squares fit. The rms error of the fit for these 50 lines is about 0.07 pixel, which corresponds to about 3 mÅ in the central parts of the spectrum (assuming a dispersion of 24 pixels Å^{-1}), or about 170 m s^{-1} in radial velocity units.

Several important points can be drawn from a careful examination of the residuals in Figure 2*c*:

1. The scatter is not random at all. Each point in the plot will keep its position relative to the zero line, as one goes from one Th-Ar image to another. Thousands of Th-Ar spectra, taken over years, always demonstrate the same distribution of the residuals as shown in Figure 2*c*. Of course, there are some random fluctuations in line positions, but they are much less (typically by a factor of 10 for strong lines). It has just been demonstrated (see Fig. 2*b*) that the strongest lines show a random scatter in position of only about 0.01 pixel. The residuals, on the other hand, are of the order of 0.1 pixel and more. One can conclude that the residuals are not a result of the measurement errors. They can be caused by some uncertainties in the laboratory wavelengths or by blending of the spectral lines. It was checked that any physical variations in pixel size or position on the CCD are negligible compared with the actual residuals.

2. The fact that the residuals are not random implies another important conclusion, namely, that the rms error of the dispersion solution (as derived from the least-squares fit) does not contribute that amount to the total random uncertainty of the radial velocity measurements, but only to the systematic error. The actual random uncertainty is much less, and it is determined by the uncertainties in the line positions (Fig. 2*b*), rather than by the residuals themselves.

3. A surprising result is also an evident systematic trend of the residuals depending on the intensities of spectral lines: the weaker the line, the larger the residual. While the strongest lines remain below the fit at about -0.1 pixel, the weakest lines seem to prefer the positive values of up to $+0.5$ pixel or so. The scatter amongst the weakest lines is much bigger, almost certainly due to their increased sensitivity to blending effects. The correlation between the residuals and the line intensities means that a different line selection necessarily leads to a different dispersion solution. A change of only 0.1 pixel in the fit, caused by the inclusion or exclusion of some weak spectral lines, will produce a velocity shift of about 240 m s^{-1}. This is another strong reason why one should always use exactly the same set of spectral lines for the wavelength calibration.

While the first two points listed above are easy to understand, the third one is somewhat more puzzling and certainly not expected. It should be emphasized here that the effect is seen only in the images using the PM3000 CCD system (Thomson chip). This result will be discussed in more detail later (see § 5). It seems that the systematic trend in the residuals (Fig. 2*c*) is neither a property of the Th-Ar spectrum nor a result of bad data reduction. Its origins can be traced deeper into the data acquisition process and are perhaps connected to the charge-transfer process during the readout cycle of the chip itself.

Using a large number of observations, a typical uncertainty of 10–15 m s^{-1} in stellar radial velocities has been found due to the dispersion solution alone. It is interesting to compare these results with a recent paper by De Cuyper & Hensberge (1998), dealing with the blending effects between close components of the thorium spectral lines, and introducing a list of adjusted wavelengths to be used for wavelength calibration purposes. With a dispersion of about 24 pixels Å^{-1} at $\lambda = 5300$ Å, the PM3000 images have an *R*-factor[3] of about 130,000. If the adjusted wave-

[2] There is no need for any higher order polynomials in this case, since they do not improve the total rms error.

[3] The *R*-factor is defined by De Cuyper & Hensberge (1998) as a ratio between the wavelength (measured in Å) and the pixel scale (measured in Å pixel^{-1}).

lengths at an R-factor of 100,000 are taken from Table 6 of De Cuyper & Hensberge (1998), one will end up with only 32 lines in the present wavelength region (instead of the 50 that are normally found). Of those 32 lines, only 10 have their adjusted wavelengths different from their standard values, and the differences are all less than 1 mÅ. The rms error of the dispersion solution, when these 32 lines are used, is about 0.06 pixel, not very much different from the usual value of 0.07 pixel. For these reasons it was decided to keep the line tables unchanged.

3.2. Synthetic Spectra and the Cross-Correlation Process

The cross-correlation technique is used to derive the radial velocities in this work. The stellar spectrum (on a logarithmic scale) is cross-correlated with a synthetic spectrum of a similar spectral type, and the velocity is derived from the position of the cross-correlation peak. The synthetic spectra have been computed especially for this project by Robert L. Kurucz, at the Harvard-Smithsonian Center for Astrophysics (R. L. Kurucz 1996, private communication). There are seven different models, as listed in Table 2. They have been computed for the standard solar metallicity, zero turbulence, and no rotation. Using the basic parameters ($T_{\rm eff}$, log g) from Table 2, the spectral types and absolute magnitudes have been derived by interpolating the data from Allen (1991).

As one might expect, the models do not match the observed spectra exactly. In general, the models are quite good for F and early-G spectral types, but not quite adequate for K and M stars. The absence of the molecular lines in the late-type synthetic spectra makes the situation even worse, especially for M stars. However, the great majority of the atomic lines are included, so that a reliable cross-correlation process and final radial velocities can be obtained. The synthetic spectral lines are all centered on the nearest bin ($\sim$0.01 Å), which sets the limit on the uncertainty of the laboratory wavelengths. However, many spectral lines are used in the cross-correlation process so that these random errors should disappear when the radial velocity derived from the whole spectral range is considered.

TABLE 2

BASIC PARAMETERS OF THE STELLAR MODELS

Model	$T_{\rm eff}$ (K)	log g	Spectral Type	M_V
f7545.....	7500	4.5	F0 V	+3.0
f6535.....	6500	3.5	F3 III	+1.3
f5525.....	5500	2.5	G1 II	−1.4
fsun	5770	4.4	G2 V	+4.8
f5045.....	5000	4.5	G9 V	+5.8
f4525.....	4500	2.5	K0 III	+0.1
f3520.....	3500	2.0	K8 III	+0.8

A test was made in order to see how the radial velocity of a star would change if a different synthetic spectrum is used (Fig. 3). The differences between the models are less than 100 m s^{-1} for similar spectral types but can be up to 200–300 m s^{-1} if the spectral types are very much different.

The cross-correlation function is computed using the fast Fourier transform (Press et al. 1994). Before the actual computation, both the synthetic and observed stellar spectra are prepared in the following way (Brault & White 1971; Simkin 1974):

1. The arithmetic mean of all pixels is computed and the mean value is subtracted from the original spectrum, so that the resulting spectrum has a zero mean.

2. A cosine bell window is applied to the spectrum, so that the intensity gradually falls toward zero at the edges. Only 20% of the pixels (10% at each end) are affected by this procedure.

The final cross-correlation functions are shown in Figure 4. A Gaussian is fitted only to the central part of a cross-correlation profile. The actual cutoff level is determined for each echelle order separately at a point where the profile starts departing from a Gaussian shape. This will not affect the final precision of the radial velocities, as long as the cutoff levels are kept exactly the same in all measurements.

There is a systematic difference between the radial velocities derived from different echelle orders. To illustrate this, many observations of β Hydri (spectral type G2 IV, synthetic spectrum fsun) have been combined and are present-

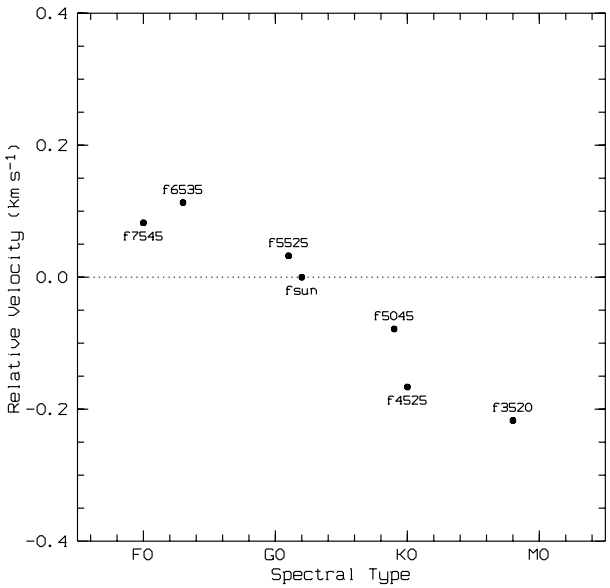

FIG. 3.—Variations in the stellar radial velocity when different synthetic spectra are used. A single sky spectrum has been correlated with the models listed in Table 2. The zero point has been set at the solar model.

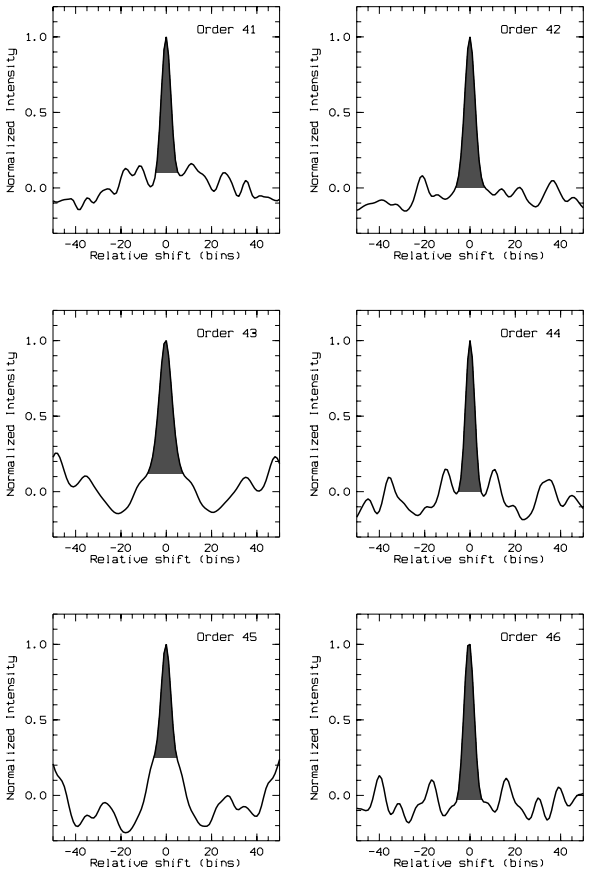

FIG. 4.—Typical cross-correlation peaks for each of the six echelle orders. Only the shaded central portions of the profiles are used for the radial velocity determinations.

ed in Figure 5. Any global variation in the radial velocity has been eliminated from each observation by subtracting the mean value from all six echelle orders. There are small random fluctuations within each order, typically around $\sigma \sim 30$–40 m s^{-1}, but the systematic shifts can be larger, up to 200–300 m s^{-1} between some orders. This is probably caused by systematic differences between the synthetic and observed spectra in different orders. A total standard deviation of ~ 100 m s^{-1} can be calculated if an average velocity is taken for each order and then all six values are combined.

4. RADIAL VELOCITIES AND PHOTON COUNTS

The reduction procedure described in § 3 should ideally lead to a radial velocity affected only by some random measurement errors, and a possible systematic error, that would shift all values by the same fixed amount with respect to the standard system. However, a surprising effect has been discovered during the data analysis in the case of the PM3000 CCD camera. It turns out that the measured radial velocities depend strongly on the actual signal levels in both the stellar and Th-Ar spectra! For example, if several Th-Ar spectra of different intensities (different exposure times) are used to reduce the same stellar spectrum, a set of different velocities will be obtained, always following the same regular pattern: the stronger the Th-Ar spectrum, the larger the velocity. It seems that the additional photons tend to move the Th-Ar spectrum to the left, producing an unwanted blueshift. In a similar way, if several stellar spectra of different signal levels are reduced using the same Th-Ar image, the radial velocity will again differ, depending on the signal level, this time demonstrating an opposite behavior: the stronger the stellar spectrum, the lower the velocity. This again means that the additional photons tend to produce a blueshift, but this time in the stellar spectrum. However, one should be more careful at this stage and allow another possibility, namely, that it might be the photon deficiency in the lower signal spectra tending to produce an unwanted redshift instead. More comments on these two alternatives will be given in § 5.

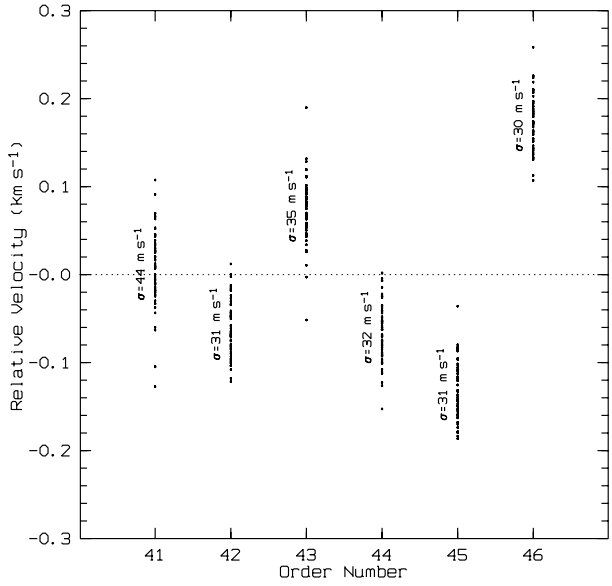

FIG. 5.—Systematic radial velocity differences between the echelle orders. The zero point of the relative velocity scale corresponds to the arithmetic mean of all six orders. The standard deviation (σ) is given for each order.

The correlation between the Th-Ar intensities and stellar radial velocities is shown in Figure 6*a*. Many observations of β Hydri and of the blue sky have been used to derive this plot. For each stellar spectrum, a set of Th-Ar spectra (all taken within an hour or so around the stellar exposure) have been used to compute the radial velocity for the star, depending on the Th-Ar intensity. The "average intensity" is defined as an arithmetic mean of the central intensities of all spectral lines used for the dispersion solution.[4] The velocities for different observations have been shifted verti-

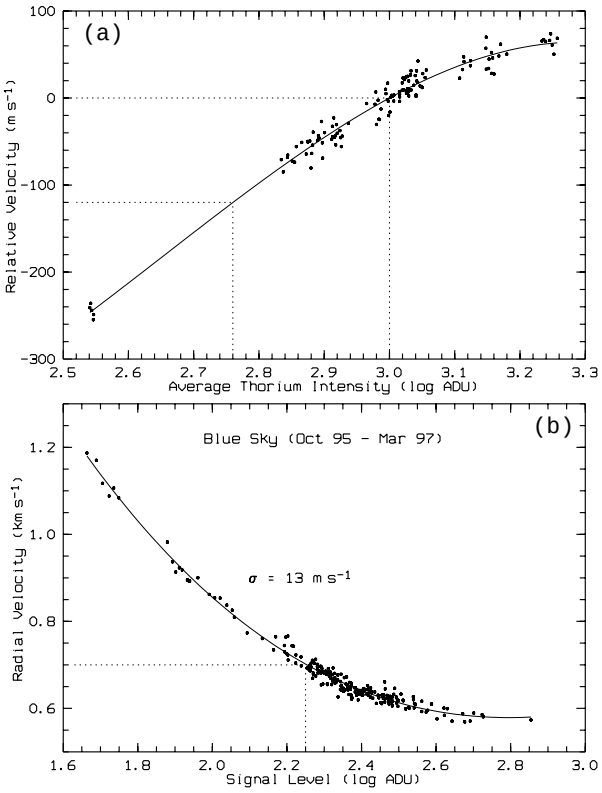

FIG. 6.—Correlation between radial velocities and (*a*) Th-Ar intensities and (*b*) stellar intensities.

cally with respect to each other, until the smallest rms error is obtained around a common smooth curve. The relative velocity scale has been centered arbitrarily at a standard Th-Ar intensity of 10^3 ADU.

The effect of stellar intensities (i.e., the number of ADU in the stellar continuum) is shown in Figure 6*b*. The signal level is defined as an average ADU count in the continuum for the whole stellar image (after the extraction of the echelle orders). Many solar spectra have been used. They have first been brought to the same Th-Ar intensity, as described above. A fixed run correction[5] has then been applied so that all data points follow a common smooth curve. This has been done in several iterations, by adjusting the run corrections each time, until the rms error reaches its minimum. A total rms error of $\sigma = 13$ m s^{-1} has been

[4] All intensities in this paper are given in ADU. To convert to electron counts an inverse gain of 4.31 e^- ADU^{-1} should be applied.

[5] Run corrections are used to account for any systematic differences between the radial velocities obtained in different observing runs. Since the optical fiber is not used by all observers, it is normally removed and reinstalled when needed. This can cause slightly different illumination of the slit. Another source of run-to-run differences is the slow deterioration of the glycerin drop at the fiber input over time (see § 2).

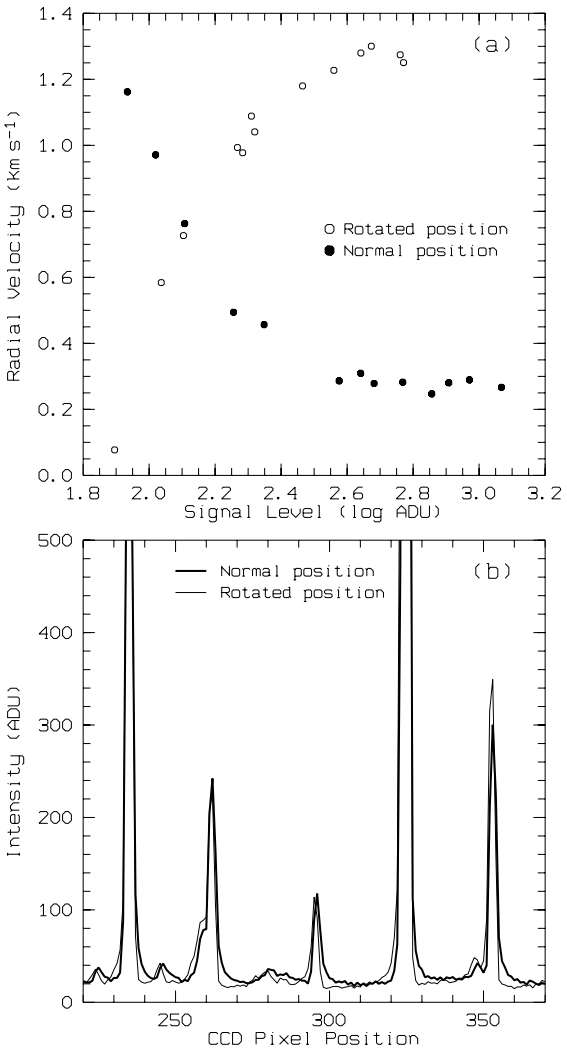

FIG. 7.—Some effects of the PM3000 CCD camera rotation on (*a*) the radial velocities and (*b*) the line profiles when the camera is rotated by 180° from its normal position.

achieved in this way over a period of 18 months. The final run corrections are typically less than ~ 50 m s^{-1}.

The transformation laws derived from Figure 6 have been used to adjust all stellar radial velocities observed with the PM3000 camera. In this way, the stellar velocities are all expressed in a system where the observed velocity of the Sun is zero. Of course, the measured radial velocity does not only reflect the motion of the star as a whole. The measurements are still affected by the gravitational redshift, as well as the convective blueshift. Only if these two effects happen to compensate each other will the results represent the true absolute radial velocities.

5. TESTING THE PM3000 CAMERA

A series of tests have been performed in order to locate the cause of the peculiar behavior of the PM3000 camera as

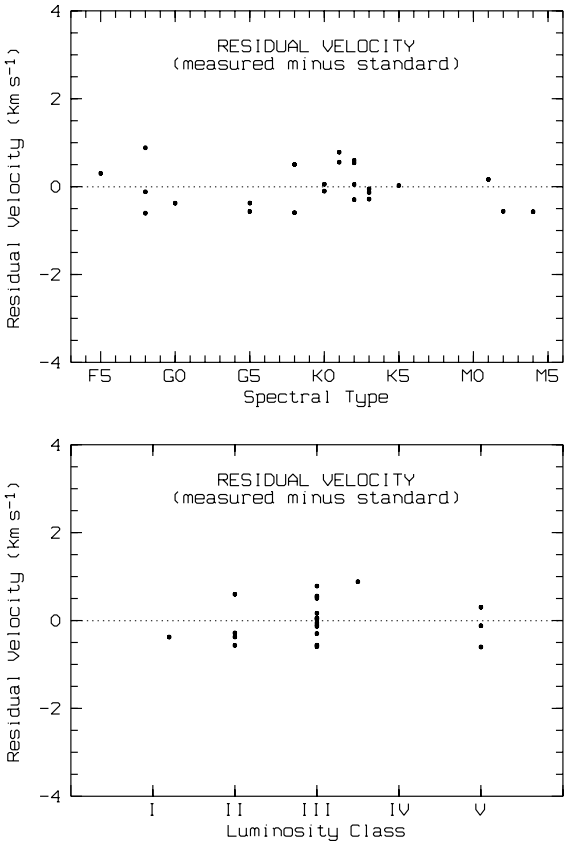

FIG. 8.—Residual velocities (measured minus standard) for the IAU standard stars, as obtained at MJUO. Each dot corresponds to a single star. The arithmetic mean is represented by a horizontal dashed line.

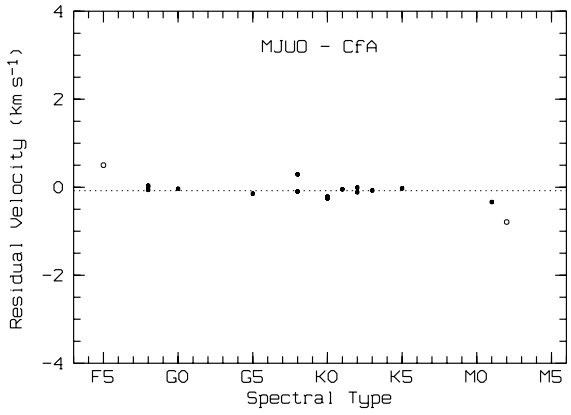

FIG. 9.—Comparison between the MJUO measurements and the CfA determinations by Stefanik et al. (1999). The mean value is represented by the dashed line. Two stars with residuals greater than 0.5 km s^{-1} (on both sides) are shown as open circles.

described in § 4. The tests consisted of blue-sky observations using different exposure times to produce different signal levels in the continuum. One-half of the observations were made with the CCD camera in its normal position. The camera was then rotated by 180° for the other half of the observations. The results are shown in Figure 7. It is obvious that the radial velocities produce a "mirror image" of their behavior when the camera is rotated (Fig. 7*a*). This means that (in the normal position) the spectra are either blueshifted at higher signal levels or redshifted at lower signal levels. A clue to distinguish between these two possibilities is found in Figure 7*b*, where an enlarged portion of the Th-Ar spectrum (around $\lambda = 5258$ Å in order 44) is presented at both camera positions. There is an asymmetry in the line profiles, mainly affecting the very bottom portions of the spectral lines and producing some "tails" departing from a Gaussian shape. The tails are seen only on one side of the profile (to the right in the normal position and to the left in the rotated position). The amount of additional ADU counts seems to be the same for all lines, independent of the central intensity. On a relative scale, the weaker lines are distorted (and redshifted) more than the stronger ones.

The reasons for such a behavior are not quite clear. The problem could be related to a poor charge-transfer efficiency. However, one would expect that the amount of charge left behind during the readout process is proportional to the charge itself, which would produce stronger tails in stronger lines. This is clearly not the case here. The problem might also be located elsewhere in the readout electronics, but investigating this would go too far from the subject of this paper. As already explained in § 4, an empirical relationship has been determined between the measured velocities and photon counts to account for this effect. The observations made with the SITe chip, however, do not suffer from this problem and no additional reduction is necessary.

6. RADIAL VELOCITIES

A number of the IAU standard radial velocity stars (Pearce 1957) have been observed (24 stars with 197 measurements in total). These observations are used to determine the zero point of the MJUO system with respect to the IAU system, as well as to check whether there are any systematic effects depending on the spectral type or the luminosity class. This is shown in Figure 8, where the residual velocity is the difference between the measured and standard values. An average value of the measured radial velocity is used for each star. The two plots demonstrate no detectable correlation between the residual velocities and either the spectral type or the luminosity class. There is a small constant offset of MJUO − IAU = −7 m s^{-1} (the arithmetic mean of all residuals) indicating that the MJUO velocities are already (within the measurement errors) in the standard IAU system. The corresponding standard devi-

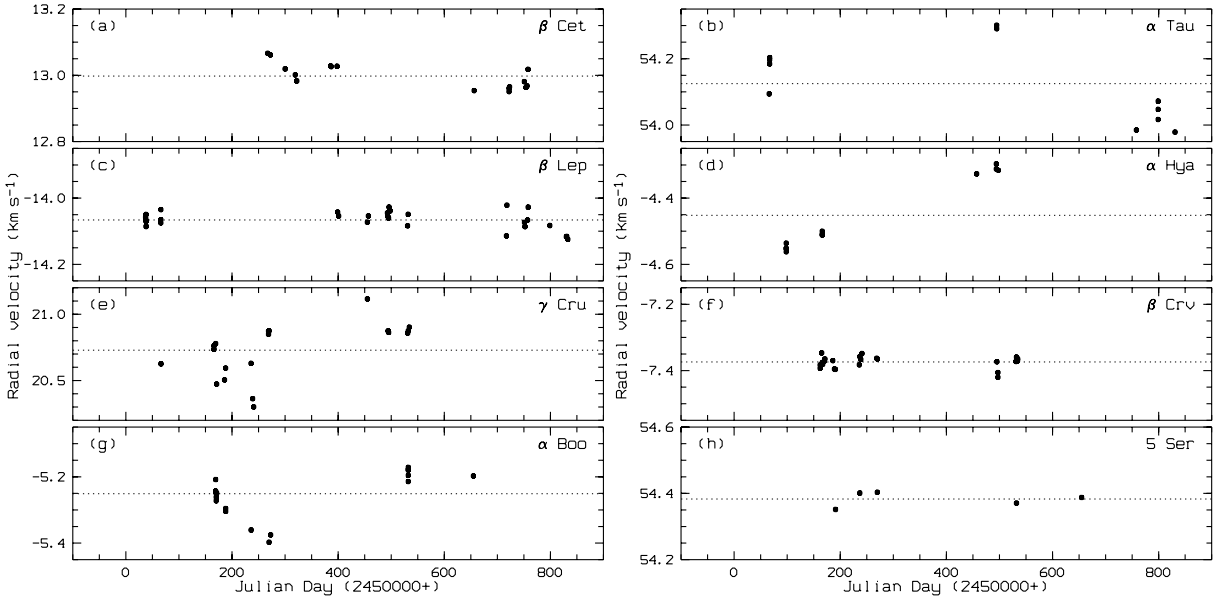

FIG. 10.—Radial velocities for some IAU standard stars as measured at MJUO. A dashed line is used to represent the mean value.

ation is $\sigma_{\mathrm{MJUO-IAU}} \approx 460$ m s^{-1}, which can be taken as a typical standard error in the absolute radial velocity for a single star. The origin of this error could be in the MJUO measurements or in the IAU system or in both.

A comparison has also been made between the MJUO measurements and a recent list of radial velocities published by Stefanik, Latham, & Torres (1999) at the Harvard-Smithsonian Center for Astrophysics (CfA). Only 17 stars are common to both the MJUO and CfA lists, and the corresponding residuals (MJUO − CfA) are shown in Figure 9. The scatter is significantly less than in Figure 8. When all 17 stars are considered, a mean residual of MJUO − CfA = −80 m s^{-1} is found with a standard deviation of $\sigma_{\mathrm{MJUO-CfA}} \approx 270$ m s^{-1}. However, when two stars with the largest residuals (0.5 km s^{-1} and above) are rejected (open circles in Fig. 9), the remaining residuals have a mean of −70 m s^{-1} with a standard deviation of only 140 m s^{-1}, which is about 3 times less than the scatter in Figure 8. This is an indication that the relatively large scatter of MJUO − CfA values could be mainly caused by errors in the IAU standard radial velocities themselves.

We can also estimate the total uncertainty of the MJUO absolute radial velocities using our measurements alone, by taking into account all the error sources described in § 3. In fact, we can consider only the two largest sources: the model mismatch for similar spectral types (∼100 m s^{-1})

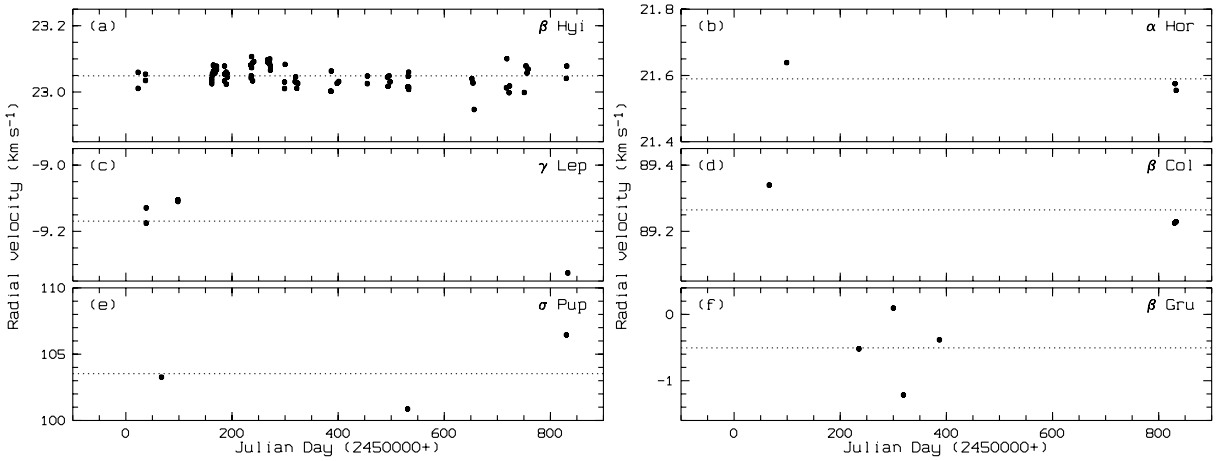

FIG. 11.—Radial velocities for some program stars as measured at MJUO. A dashed line is used to represent the mean value.

and order-to-order differences ($\sim$100 m s^{-1}), while the other random effects are small enough to be neglected. We obtain $\sigma_{abs} \approx (100^2 + 100^2)^{1/2}$ ms$^{-1} \approx 140$ ms^{-1}, which is in reasonable agreement with the above values derived from the MJUO $-$ CfA difference. We can conclude that the MJUO absolute radial velocities have an uncertainty of about 100–200 m s^{-1}.

Some of the standard stars measured at MJUO (those observed three or more times) are presented in Table 3 and in Figure 10. The standard deviation (tabulated as σ) represents the standard error of one observation (not the standard error of the mean) and includes the random measurement errors and any intrinsic variability in the stellar radial velocity. The CfA values by Stefanik et al. (1999) are also given in Table 3 for comparison. Most of the standard stars exhibit some level of variability, confirming numerous results already published by other authors. However, there are examples of extremely stable velocities, with standard deviations as small as 20–30 m s^{-1}. In particular, this is the case with the two G5 II standards, β Leporis and β Corvi (Figs. 10*c* and 10*f*). Another example is 5 Ser (spectral type F8 III–IV) in Figure 10*h* with a standard deviation of 22 m s^{-1}, but with only five measurements. On the other hand, the standard deviation for Arcturus (69 m s^{-1}) indicates a possible variability, which is in agreement with other published results. For example, an amplitude of 160 m s^{-1} was reported by Smith, McMillan, & Merline (1987) and another one of about 100 m s^{-1} by Hatzes & Cochran (1993). These amplitudes would correspond to somewhat lower standard deviations that would not be significantly different from our value.

Velocities of some program stars (those observed three or more times) are presented in Table 4 and in Figure 11. By far the most frequently observed program star is β Hydri, a bright southern circumpolar subgiant (Fig. 11*a*). There are 80 observations of this star demonstrating a fairly constant

TABLE 3

IAU Standard Radial Velocity Stars

HD	Name	m_v	Spectral Type	Interval (days)	N	V_r (km s^{-1})	σ (km s^{-1})	V_r(CfA) (km s^{-1})	σ(CfA) (km s^{-1})
4128	β Cet	2.0	K0 III	491	16	12.998	0.038	13.25	0.41
29139	α Tau	0.9	K5 III	765	11	54.125	0.117	54.15	0.41
36079	β Lep	2.8	G5 II	796	33	$-$14.066	0.026	$-$13.92	0.31
81797	α Hya	2.0	K3 III	400	11	$-$4.452	0.112	$-$4.38	0.46
108903.....	γ Cru	1.6	M4 III	468	19	20.729	0.209	...	...
109379.....	β Crv	2.6	G5 II	372	26	$-$7.374	0.017	...	...
124897.....	α Boo	$-$0.1	K2 IIIp	486	19	$-$5.251	0.069	$-$5.14	0.42
136202.....	5 Ser	5.1	F8 III–IV	464	5	54.383	0.022	54.35	0.44
146051.....	δ Oph	2.7	M1 III	365	7	$-$19.635	0.113	$-$19.30	0.47
150798.....	α TrA	1.9	K2 IIb–IIIa	492	12	$-$3.103	0.113	...	...
157457.....	κ Ara	5.2	K1 III	106	6	17.957	0.050	...	...
161096.....	β Oph	2.8	K2 III	479	3	$-$12.297	0.020	$-$12.29	0.42
168454.....	δ Sgr	2.7	K3 III	465	5	$-$20.133	0.139	...	...
204867.....	β Aqr	2.9	G0 Ib	658	12	6.324	0.143	6.36	0.56

TABLE 4

Program Stars

HD	Name	m_v	Spectral Type	Interval (days)	N	V_r (km s^{-1})	σ (km s^{-1})
2151	β Hyi	2.8	G2 IV	808	80	23.049	0.031
26967	α Hor	3.9	K1 III	734	3	21.590	0.044
38393	γ Lep	3.6	F7 V	795	5	$-$9.169	0.092
39425	β Col	3.1	K1.5 III	767	3	89.265	0.065
59717	σ Pup	3.2	K5 III SB	763	3	103.528	2.803
93497	μ Vel	2.7	G5 III SB	368	4	6.506	0.011
100407.....	ξ Hya	3.5	G8 III	73	3	$-$4.792	0.040
120452.....	89 Vir	5.0	K0 III	334	3	$-$39.598	0.018
148786.....	φ Oph	4.3	G8/K0 III	489	3	$-$33.988	0.054
183275.....		5.5	K1/K2 III	417	3	$-$31.404	0.144
214952.....	β Gru	2.2	M5 III	152	4	$-$0.505	0.541

radial velocity over an interval of about 800 days, with a standard deviation of only 31 m s^{-1}. Most of the other stars have their uncertainties less than 100 m s^{-1}. Unfortunately, there are not enough observations to investigate any possible variability of these stars in a more adequate way. However, two of the program stars (σ Puppis in Fig. 11*e* and β Gruis in Fig. 11*f*) show variations large enough to be classified as RV variable stars.

This work has been supported by the University of Canterbury Doctoral Scholarship, the Royal Society of New Zealand 1996 R. H. T. Bates Postgraduate Scholarship, and a Marsden Fund grant. The authors would like to thank Robert L. Kurucz (Harvard-Smithsonian Center for Astrophysics) for providing the synthetic stellar spectra used in this work.

REFERENCES

Allen, C. W. 1991, Astrophysical Quantities (3d ed.; London: Athlone)
Baranne, A., et al. 1996, A&AS, 119, 373
Brault, J. W., & White, O. R. 1971, A&A, 13, 169
Brown, T. M., Noyes, R. W., Nisenson, P., Korzennik, S. G., & Horner, S. 1994, PASP, 106, 1285
Cummings, I. N. 1998, Ph.D. thesis, Univ. Canterbury
De Cuyper, J.-P., & Hensberge, H. 1998, A&AS, 128, 409
Gray, D. F., Tycner, C., & Brown, K. 2000, PASP, 112, 328
Hatzes, A. P., & Cochran, W. D. 1993, ApJ, 413, 339
Hearnshaw, J. B. 1977, Proc. Astron. Soc. Australia, 3, 102
Kershaw, G. M., & Hearnshaw, J. B. 1989, Southern Stars, 33, 89
Marcy, G. W., Butler, R. P., & Fischer, D. A. 1999, in IAU Colloq. 170, Precise Stellar Radial Velocities, ed. J. B. Hearnshaw & C. D. Scarfe (ASP Conf. Ser. 185; San Francisco: ASP), 121
Murdoch, K. A., Hearnshaw, J. B., & Clark, M. 1993, ApJ, 413, 349
Palmer, B. A., & Engleman, R., Jr. 1983, Atlas of the Thorium Spectrum (LA-9615; Los Alamos: Los Alamos National Lab.)
Pearce, J. A. 1957, Trans. IAU, 9, 441
Press, W. H., Teukolsky, S. A., Vetterling, W. T., & Flannery, B. P. 1994, Numerical Recipes in C: The Art of Scientific Computing (2d ed.; Cambridge: Cambridge Univ. Press)
Reader, J., & Corliss, C. H. 1980, Wavelengths and Transition Probabilities for Atoms and Atomic Ions, Part I. Wavelengths (NSRDS-NBS 68; Washington, DC: US Government Printing Office)
Simkin, S. M. 1974, A&A, 31, 129
Skuljan, J., Cottrell, P. L., & Hearnshaw, J. B. 1997, Proc. ESA Symp. *Hipparcos*-Venice '97 (ESA SP-402; Noordwijk: ESA), 525
Skuljan J., Hearnshaw, J. B., & Cottrell, P. L. 1999a, in IAU Colloq. 170, Precise Stellar Radial Velocities, ed. J. B. Hearnshaw & C. D. Scarfe (ASP Conf. Ser. 185; San Francisco: ASP), 91
———. 1999b, in IAU Colloq. 170, Precise Stellar Radial Velocities, ed. J. B. Hearnshaw & C. D. Scarfe (ASP Conf. Ser. 185; San Francisco: ASP), 98
———. 1999c, MNRAS, 308, 731
Smith, P. H., McMillan, R. S., & Merline, W. J. 1987, ApJ, 317, L79
Stefanik, R. P., Latham, D. W., & Torres, G. 1999, in IAU Colloq. 170, Precise Stellar Radial Velocities, ed. J. B. Hearnshaw & C. D. Scarfe (ASP Conf. Ser. 185; San Francisco: ASP), 354
Tobin, W. 1992, Southern Stars, 34, 421